Letter

Tracking chirality in photoelectron circular dichroism

Marec W. Heger and Daniel M. Reich*
Dahlem Center for Complex Quantum Systems and Fachbereich Physik, Freie Universität Berlin, Arnimallee 14, D-14195 Berlin, Germany

(Received 1 July 2024; revised 26 November 2024; accepted 31 January 2025; published 28 February 2025)

In photoelectron circular dichroism (PECD) it is generally difficult to trace how and when the chirality of the molecule is imprinted onto the photoelectron. We present simulations of PECD in a simple model and employ chirality measures to establish a quantitative connection between the chirality of the potential, the electronic wave function's chirality, and the anisotropy of the photoelectron distribution. We show that these measures are suitable indicators for chirality, paving the way for tracking the chiral evolution from the nuclear scaffold to the final observable.

DOI: 10.1103/PhysRevResearch.7.L012047

Chiral molecules play an important role in biology, chemistry, and physics [1–5] since their handedness prominently affects interactions with chiral light and matter. A chiral nuclear scaffold gives rise to a chiral potential and imprints a notion of handedness on the system which can be probed and measured via suitable observables. Prominent examples for such observables are microwave three-wave mixing [6–13], circular dichroism (CD) [14–19], and photoelectron circular dichroism (PECD) [20–28], with the latter allowing for large anisotropies in many molecular species. While it has been shown that PECD in the gas phase is strongly affected by short-range interactions [29], it was recently demonstrated that even in a hydrogen atom, excitations to chiral intermediate states lead to a PECD signal despite the absence of a chiral short-range potential [30]. This highlights the complex interplay of the nuclear geometry, the initial electronic wave function, and the interaction with the circularly polarized driving field.

In general, the initial state inherits its chirality from the nuclear scaffold, which underlines the importance of geometric properties for generating chiral signatures. Candidates for geometric measures to quantify chirality were previously suggested [30–36] for, e.g., electron wave functions and densities, point mass distributions, photoelectron distributions, as well as electric fields. However, the application of such measures as a tool to elucidate the connection between the chirality of the nuclear scaffold, respectively the electronic wave function, and experimental chiral observables has so far been missing.

In this Letter, we employ chirality measures for potentials and wave functions. We analyze their ability to track the emergence of PECD as a paradigmatic chiral observable and conduct an investigation into how far such measures can be used to predict the strength of PECD. To keep the chiral system in our study as simple and tunable as possible, we consider single-photon ionization of hydrogen subject to an artificial chiral potential. This potential mimics the local chiral environment of electrons in PECD experiments. Time-dependent simulations of the electron dynamics demonstrate a qualitative and quantitative link between the anisotropy in the photoelectron distribution and the chirality measures for the potential and the electronic wave function.

We employ the Hamiltonian

$$H(t) = H_{\mathrm{H}} + gV_{\mathrm{chiral}} + \boldsymbol{A}(t)\cdot\boldsymbol{p}, \tag{1}$$

with H_{H} the Hamiltonian of atomic hydrogen, V_{chiral} an artificial chiral potential with a scaling factor g, and $\boldsymbol{A}(t)\cdot\boldsymbol{p}$ the interaction with a laser field in the electric dipole approximation using the velocity gauge. The potential V_{chiral} introduces chirality to the system. We expand it in real-valued spherical harmonics Y_{lm}, i.e.,

$$V_{\mathrm{chiral}} = V(r)\sum_{lm} c_{lm}Y_{lm}(\varphi,\theta), \tag{2}$$

with expansion coefficients c_{lm}. This simple model allows us to systematically tune the system's chirality. Our study is focused on the angular dependence which plays the critical role in breaking inversion symmetry. To this end, we treat the radial dependence $V(r)$ as a simple prefactor for the spherical harmonic expansion, thus limiting any chirality to emerge from the chiral potential via the c_{lm}. $V(r)$ is chosen as a screened Coulomb potential with a screening length of 0.21 nm, localizing the effect of the potential around the center. This screening together with the hydrogenic nature of our system is reminiscent of tightly bound K-shell electrons in a chiral molecule's chiral center.

We study different potentials V_{chiral} by truncating the expansion in l according to Eq. (2) at different values. We call this truncation threshold L. A restriction to low values of L allows us to construct chiral potentials via a simple spherical harmonics expansion featuring only few coefficients. A similar low-order expansion for states has been applied to study the propensity rules in PECD [37]. Although in realistic

*Contact author: danreich@zedat.fu-berlin.de

chiral molecules much higher orders in L will commonly be involved [38], electromagnetic potentials with low L can be artificially engineered via generating low-order multipole moments using static electric fields [39]. When imprinting chirality in such an external fashion, one could mimic random orientations of molecules in the gas phase by rotating the fields with respect to the ionizing pulse. Note, however, that the radial dependence of the potential in such a framework would differ from the screened Coulomb profile in our model.

In photoelectron circular dichroism the system's chirality is probed via ionization using a circularly polarized light field [cf. the final term in Eq. (1)]. This leads to a forward-backward asymmetry of photoelectrons even for randomly oriented molecular targets. For simplicity, we restrict ourselves to single-photon ionization in this study. To simulate the PECD we solve the time-dependent Schrödinger equation (TDSE) utilizing the Runge-Kutta propagator. We represent the angular degree of freedom of the electronic wave function via spherical harmonics and the radial degree of freedom via a Gauss-Lobatto finite-element discrete variable representation [40,41]. The photoelectron spectra are continuously extracted during time evolution using the time-dependent surface flux method (t-SURFF) [42,43]. Furthermore, we employ a complex absorbing potential (CAP) [44] to avoid unphysical reflections. To simulate PECD in the gas phase we need to account for arbitrary orientations of the chiral potential with respect to the propagation direction of the laser field. We calculate the photoelectron spectra of multiple individual orientations obtained by rotating V_{chiral} via the Euler angles $\alpha\beta\gamma$. Since every orientation requires a full propagation of the laser-induced dynamics, we use the efficient Lebedev scheme [45] to keep the numerical effort low.

To quantify and track how the chirality of the molecular potential is reflected in the electronic wave function we employ a chirality measure expanding the scope of previous suggestions [30–34]. We emphasize that any chirality measure should ensure that achiral objects are mapped to a value of zero and chiral objects to a nonzero value. To this end, we need to distinguish the quantification of chirality for potentials and wave functions. For the case of potentials—or, more generally, real-valued scalar functions $f(\boldsymbol{r})$—we define

$$\chi^{\text{V}}(f(\boldsymbol{r})) = \frac{\min_{\alpha\beta\gamma} \int_{\mathbb{R}^3} |R^{\alpha\beta\gamma} P f^c(\boldsymbol{r}) - f^c(\boldsymbol{r})|^2 d^3r}{4 \int_{\mathbb{R}^3} |f(\boldsymbol{r})|^2 d^3r}. \quad (3)$$

The idea of Eq. (3) is to find the minimal overlap between $f^c(\boldsymbol{r})$ and its mirror image $Pf^c(\boldsymbol{r})$ via arbitrary rotations $R^{\alpha\beta\gamma}$ in a proper frame of reference. To perform the rotations in such a frame we define $f^c(\boldsymbol{r}) = Tf(\boldsymbol{r})$ with T a translation such that the first moment of $|f^c(\boldsymbol{r})|^2$ is zero. It is critical to evaluate the minimization over all rotations in a suitable frame of reference. This is because a chirality measure which only minimizes over all rotations in an arbitrary frame can lead to achiral objects being assigned a nonzero value. One can avoid this issue altogether by performing a minimization over all translations on top of the rotations [31], however, this is impractical. An alternative approach [34] is to evaluate the measures with minimization only over rotations in a coordinate system where the first moment, i.e., the "center of mass," of $|f(\boldsymbol{r})|^2$ vanishes. In the Supplemental Material [46] we prove that in such a frame of reference the chirality measure from Eq. (3) is guaranteed to yield $\chi = 0$ for achiral objects even when only minimizing over the set of rotations. Our proof also demonstrates that chiral objects are guaranteed to yield nonzero chirality measure. Moreover, the resulting value of χ will always be an upper bound to a chirality measure which includes minimization over both rotations and translations.

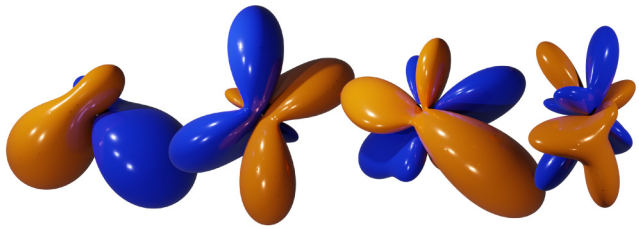

L	2	3	4	5
χ^{V}	0.10	0.25	0.28	0.33

FIG. 1. Isosurfaces with values −0.22 (blue) and 0.22 (orange) for chiral potentials according to Eq. (2) with optimized coefficients c_{lm} for angular expansions up to $L = 2$–5 and $g = 0.747$. The value of the chirality measure according to Eq. (3) is indicated below each potential.

Equation (3) cannot be used as a chirality measure for wave functions. This is because states which differ only by a global phase would not be treated equivalently by the above definition. To amend this, we represent the state as a density matrix to ensure that any global phase has no impact on the chirality measure,

$$\chi^{\rho}(\rho) = \frac{\min_{\alpha\beta\gamma} \|R^{\alpha\beta\gamma} P \rho^c P^\dagger R^{\alpha\beta\gamma\dagger} - \rho^c\|_{\text{HS}}^2}{2\|\rho\|_{\text{HS}}^2}. \quad (4)$$

Here, $\|\cdot\|_{\text{HS}}$ is the Hilbert-Schmidt norm. Following an analogous approach to Eq. (3), a proper frame of reference is chosen by employing ρ^c which is obtained from the density matrix ρ via a translation to a frame in which the first moment, i.e., the position expectation value, is zero. This guarantees that χ^{ρ} is zero if and only if the state is an achiral object. The measures from Eqs. (3) and (4) are normalized such that they take values in the interval [0,1]. We highlight that both measures are scalar—not pseudoscalar—quantities. This avoids the occurrence of chiral zeros [47]. This comes at the cost of not being able to characterize the handedness of an object, since, e.g., two enantiomeric forms of a chiral object are mapped to the same value.

Recently, it was shown that optimizing the nuclear scaffold in a model system allows to maximize PECD [48]. Instead of directly using the observable as the figure of merit, we consider in our simulations optimized angular chiral potentials with respect to the geometric notion of chirality as quantified by the chirality measure χ^{V} from Eq. (3) (see Supplemental Material [46] for details). The potentials we obtain are thus optimized independently of a particular observable yet still allow us to ascertain how the inherent chirality of the molecular structure is reflected in PECD. Our results are visualized in Fig. 1. We observe that for a larger truncation limit L, the attainable values of χ^{V} increase as well. This is because a

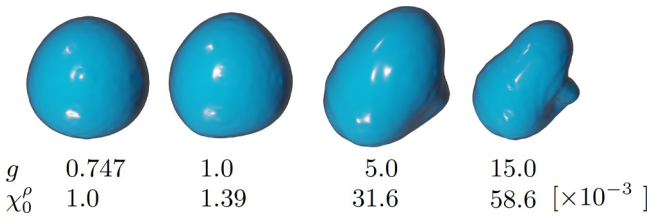

FIG. 2. Isosurfaces with value 0.03 of the ground-state electron density for the optimized $L = 3$ chiral potential and different strengths g. The value of the chirality measure according to Eq. (4) is shown below each state.

larger value of L allows for more parameters and thus degrees of freedom which can be explored during the optimization.

The potential imprints chirality onto the electron, which is often prominently reflected in the ground-state wave function $|\psi_0\rangle$. The connection between potential and ground state is particularly direct for small chiral strengths g where the chiral potential can be considered as a perturbation to the achiral H_H [cf. Eq. (1)]. In the Supplemental Material [46] we show via perturbation theory that to leading order this leads to a chirality measure of the ground state χ_0^ρ which is proportional to g^2. In the perturbative regime, increasing g thus directly translates to scaling the chirality of the system. Figure 2 visualizes the gradual deformation of the ground-state electron density for the $L = 3$ chiral potential for increasing g, illustrating how the chirality measure for states, Eq. (4), captures this increase. For small g the ground state is predominantly of s type, with increasing contributions from p and d orbitals for larger values of g. For increasing values of g the electron density starts to follow the attractive (blue) part of the chiral potential (cf. Fig. 1). In all simulations of PECD throughout this Letter we ensured to remain in the regime where the chiral potential can be seen as a perturbation. This is a realistic assumption for, e.g., the local chiral potentials of K-shell electrons in chiral molecules which inspired our model.

We employ the chirality measure to track the dynamic evolution of chirality. To this end, we average the chirality measure for the electronic wave function over all orientations at time t, denoting the rotationally averaged chirality measure $\bar{\chi}_t^\rho$. Figure 3 shows $\bar{\chi}_t^\rho$ for the time-dependent wave function using the $L = 3$ chiral potential with $g = 0.747$ (cf. Fig. 1). The ionizing pulse is circularly polarized with a duration of 2.41 fs, a wavelength of 45.5 nm, and a sine-squared temporal envelope with an amplitude of 5×10^9 V/m. The ionization yield obtained by this pulse is shown in Fig. 3(a). The 1-σ standard deviation for $\bar{\chi}_t^\rho$ over all orientations is indicated by the orange-shaded area. Furthermore, we show the orientationally averaged chirality measure of the continuum part of the electronic wave function only (blue). This continuum part is obtained via projection of the total wave packet onto the set of field-free energy eigenstates, obtained by diagonalizing $H_\mathrm{H} + gV_\mathrm{chiral}$, and subsequent removal of all wave-packet components with a negative eigenvalue. Analogously, the light-blue shaded area displays the 1-σ standard deviation for the continuum electron. The time-dependent Cartesian components of the pulse in the polarization plane are shown in Fig. 3(b). We find that the chirality measure of the time-dependent electronic wave function steadily increases during

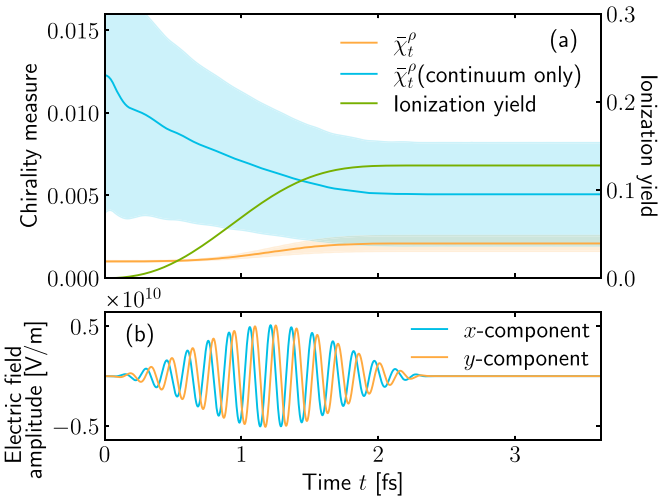

FIG. 3. (a) Orientationally averaged chirality measure of the time-evolved state (orange) and for only the continuum part of the electronic wave function (blue) for the optimized $L = 3$ potential with $g = 0.747$, and total ionization yield (green). The light-orange shaded area shows the 1-σ deviation of the chirality measure for the time-evolved state among all orientations. The light-blue shaded area analogously shows the 1-σ deviation for the continuum state. (b) Electric field components of the circularly polarized pulse in the polarization plane.

the ionization, reaching a final-time value larger than the chirality measure of the ground state. This trend is not limited to the $L = 3$ potential but can be observed for all optimized potentials we studied in the perturbative regime (data not shown). The chirality measure for the continuum part of the electronic wave function shows a large onset chirality which steadily decreases as the electron moves out of the chiral potential. The value at final time is, however, still larger than the chirality of the total wave function, highlighting the role of the continuum in manifesting the chiral signature. We attribute the large initial values for the chirality measure to the fact that the electron still remains close to the chiral center and thus inside the chiral potential at early times. An appreciable part of this chirality is lost once the electron propagates outward such that it can be interpreted as "transient chirality." For large times, only the nontransient chirality remains, as tracked by the convergence of our chirality measure to an asymptotic value and it is only this chirality which is captured in the photoelectron angular distribution and thus the PECD signal. Details on our analysis of the transient chirality are provided in the Supplemental Material [46].

We also investigate whether chirality of the ground state and of the electronic wave function can be related to the strength of the chiral observable, i.e., the PECD signal. The PECD signal can be characterized by expanding the orientationally averaged photoelectron angular distribution via odd Legendre coefficients c_i, which gives rise to the so-called linear PECD (LPECD) [51]. The c_i are generally energy dependent—we consider their values at the ionization peak. Since we study single-photon ionization, only c_1 contributes to the expansion [49], i.e.,

$$\mathrm{LPECD} = \frac{1}{c_0}\left(2c_1 - \frac{1}{2}c_3 + \frac{1}{4}c_5 + \cdots\right) \xrightarrow{1\,\mathrm{ph.}} \frac{2c_1}{c_0}, \quad (5)$$

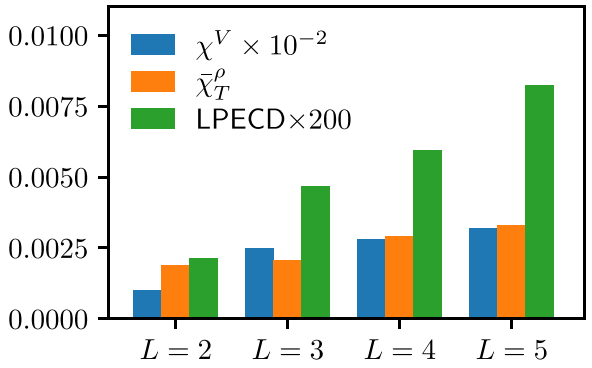

FIG. 4. Chirality measure for the potential, the wave function at final time, and LPECD for optimized potentials with different values of L (cf. Fig. 1). The potential scaling factor g is chosen such that $\chi_0^\rho = 10^{-3}$ throughout.

with c_0 the total ionization signal. Note that in order to ensure a fair comparison we tuned the pulse frequency such that the photoelectron peak position consistently stays at 13.6 eV for all chiral potentials. We provide further details in the Supplemental Material [46]. To separate the emergence of chirality in the ionization process from the chirality of the initial ground state, we adjust the strength of the chiral potential g in all simulations such that the chirality measure of the ground state is kept at a constant value of 10^{-3}. Concretely, this requires g to be increased for potentials with a higher L cutoff. We attribute this to the fact that spherical harmonics with higher l have a diminished influence on the ground state due to the larger energetic distance from the ground state. This leads to a reduced imprint of the chiral potential onto the ground state for these higher-order terms.

Figure 4 shows the orientationally averaged chirality measure of the wave function at final time $\bar{\chi}_T^\rho$, the chirality measure of the potential χ^V, and the value of the resulting LPECD. Strikingly, Fig. 4 demonstrates that all chiral quantities move in tandem with increasing L. This is a strong indicator for the predictiveness of the chirality measures for both the potential and the final state in terms of the experimentally observable chiral signature. In addition to the results shown in Fig. 4 we performed further simulations adjusting the pulse frequency to shift the photoelectron peak to 10.9, 20.4, and 27.2 eV. All calculations displayed the same qualitatively and quantitatively behavior discussed previously, i.e., a steady increase in LPECD for potentials with higher L with a larger chirality measure for the states at final time. Thus, our results extend to a broad range of photoelectron energies. Nevertheless, we expect that the predictiveness of our chirality measures will have some limits. For example, in our model the chiral potential acts only perturbatively on both bound and continuum states of a hydrogenic system. This leads to a ground state with strong s-type character. Since we consider a single-photon ionization process, the most important part of the continuum are states with a predominant p character. If a chiral potential has large coefficients for $l = 1$ this can potentially lead to a higher "effective" chirality for such states which is not distinguished from higher l contributions by the measure. Similarly, although PECD from excited states goes beyond the scope of this Letter, ionization from other initial states featuring, e.g., p- or d-type character will likely alter the effect of the chiral potential on the electron appreciably, for example, by affecting the population of individual partial waves in the continuum. Even for the ionization from the ground state studied in this Letter, we found that for potentials with higher L a trend toward populating higher partial waves in the continuum can be observed. As a result, we attribute the larger values of the chirality measure for the electronic state at final time at least partially to higher angular momentum contributions, similarly to the increased chirality measures for the potential which can be attained with larger truncation thresholds L.

In conclusion, we have shown in a simple model that chirality measures for potentials and wave functions can be used as a tool to track the emergence and predict the strength of chiral observables, such as PECD. Specifically, a large chirality measure of the potential directly translates into a large chirality measure for the ground states and eventually a large PECD signal in our simulations. We emphasize that chirality measures need to be adapted to the physical problem. For example, to guarantee that achiral objects are assigned a chirality measure of zero it is important to account for all rotations *and* translations or at least to move to a proper frame of reference. Further development of the chirality measures toward fully taking into account translations will be subject to future work. Although no single measure of chirality can be expected to be a perfect quantitative predictor for arbitrary chiral observables, the performance of the chirality measures in the examples we studied here is encouraging in terms of their potential applicability in a wider range of systems and for other chiral observables such as, e.g., circular dichroism.

We would like to thank Christiane Koch, Raoul Ebeling, Alexander Blech, and Bar Ezra for helpful discussions. Financial support by the Deutsche Forschungsgemeinschaft (DFG, German Research Foundation)–Project-ID 328961117-SFB 1319 is gratefully acknowledged.

[1] B. Ritchie, Theoretical studies in photoelectron spectroscopy: Use of angular distribution data to deduce molecular orbital parameters, III. Extraction of effective charge and anisotropy parameters of the molecular orbital from energy dependent measurements of β, the asymmetry parameter of the angular distribution, J. Chem. Phys. **61**, 3291 (1974).

[2] T. C. Johnstone and S. J. Lippard, The chiral potential of phenanthriplatin and its influence on guanine binding, J. Am. Chem. Soc. **136**, 2126 (2014).

[3] A. Comby, S. Beaulieu, M. Boggio-Pasqua, D. Descamps, F. Légaré, L. Nahon, S. Petit, B. Pons, B. Fabre, Y. Mairesse, and V. Blanchet, Relaxation dynamics in photoexcited

chiral molecules studied by time-resolved photoelectron circular dichroism: Toward chiral femtochemistry, J. Phys. Chem. Lett. **7**, 4514 (2016).

[4] I. Deveson, B. Madala, J. Blackburn, C. Barker, T. Wong, K. Barton, M. Smith, D. N. Watkins, and T. Mercer, Chiral DNA sequences as commutable controls for clinical genomics, Nat. Commun. **10**, 1342 (2019).

[5] M. H. M. Janssen and I. Powis, Detecting chirality in molecules by imaging photoelectron circular dichroism, Phys. Chem. Chem. Phys. **16**, 856 (2014).

[6] M. Leibscher, J. Kalveram, and C. P. Koch, Rational pulse design for enantiomer-selective microwave three-wave mixing, Symmetry **14**, 871 (2022).

[7] W. Sun and M. Schnell, Microwave three-wave mixing spectroscopy of chiral molecules in weakly bound complexes, J. Phys. Chem. Lett. **14**, 7389 (2023).

[8] D. Patterson, M. Schnell, and J. M. Doyle, Enantiomer-specific detection of chiral molecules via microwave spectroscopy, Nature (London) **497**, 475 (2013).

[9] V. A. Shubert, D. Schmitz, D. Patterson, J. M. Doyle, and M. Schnell, Identifying enantiomers in mixtures of chiral molecules with broadband microwave spectroscopy, Angew. Chem., Int. Ed. **53**, 1152 (2014).

[10] S. Lobsiger, C. Perez, L. Evangelisti, K. K. Lehmann, and B. H. Pate, Molecular structure and chirality detection by Fourier transform microwave spectroscopy, J. Phys. Chem. Lett. **6**, 196 (2015).

[11] J. H. Lee, J. Bischoff, A. O. Hernandez-Castillo, B. Sartakov, G. Meijer, and S. Eibenberger-Arias, Quantitative study of enantiomer-specific state transfer, Phys. Rev. Lett. **128**, 173001 (2022).

[12] H. Singh, F. E. L. Berggötz, W. Sun, and M. Schnell, Chiral control of gas-phase molecules using microwave pulses, Angew. Chem., Int. Ed. **62**, e202219045 (2023).

[13] S. R. Domingos, C. Pérez, M. D. Marshall, H. O. Leung, and M. Schnell, Assessing the performance of rotational spectroscopy in chiral analysis, Chem. Sci. **11**, 10863 (2020).

[14] C. Logé and U. Boesl, Multiphoton ionization and circular dichroism: New experimental approach and application to natural products, ChemPhysChem **12**, 1940 (2011).

[15] M. Stener, D. D. Tommaso, G. Fronzoni, P. Decleva, and I. Powis, Theoretical study on the circular dichroism in core and valence photoelectron angular distributions of camphor enantiomers, J. Chem. Phys **124**, 024326 (2006).

[16] A. Rizzo, N. Lin, and K. Ruud, *Ab initio* study of the one- and two-photon circular dichroism of *R*-(+)-3-methylcyclopentanone, J. Chem. Phys **128**, 164312 (2008).

[17] F. Pulm, J. Schramm, J. Hormes, S. Grimme, and S. D. Peyerimhoff, Theoretical and experimental investigations of the electronic circular dichroism and absorption spectra of bicyclic ketones, Chem. Phys. **224**, 143 (1997).

[18] A. Bornschlegl, C. Logé, and U. Boesl, Investigation of CD effects in the multi photon ionisation of R-(+)-3-methylcyclopentanone, Chem. Phys. Lett. **447**, 187 (2007).

[19] N. Berova, K. Nakanishi, and R. W. Woody, *Circular Dichroism: Principles and Applications*, 2nd ed. (Wiley, Hoboken, NJ, 2000).

[20] I. Powis, Photoelectron circular dichroism in chiral molecules, in *Advances in Chemical Physics*, edited by S. A. Rice (Wiley, Hoboken, NJ, 2008), Vol. 138, Chap. 5, pp. 267–329.

[21] C. Lux, M. Wollenhaupt, T. Bolze, Q. Liang, J. Köhler, C. Sarpe, and T. Baumert, Circular dichroism in the photoelectron angular distributions of camphor and fenchone from multiphoton ionization with femtosecond laser pulses, Angew. Chem., Int. Ed. **51**, 5001 (2012).

[22] A. Kastner, C. Lux, T. Ring, S. Züllighoven, C. Sarpe, A. Senftleben, and T. Baumert, Enantiomeric excess sensitivity to below one percent by using femtosecond photoelectron circular dichroism, ChemPhysChem **17**, 1119 (2016).

[23] R. Cireasa, A. E. Boguslavskiy, B. Pons, M. C. H. Wong, D. Descamps, S. Petit, H. Ruf, N. Thiré, A. Ferré, J. Suárez, J. Higuet, B. E. Schmidt, A. F. Alharbi, F. Légaré, V. Blanchet, B. Fabre, S. Patchkovskii, O. A. Smirnova, Y. Mairesse, and V. R. Bhardwaj, Probing molecular chirality on sub-femtosecond timescale, Nat. Phys. **11**, 654 (2015).

[24] D. Faccialà, M. Devetta, S. Beauvarlet, N. Besley, F. Calegari, C. Callegari, D. Catone, E. Cinquanta, A. G. Ciriolo, L. Colaizzi, M. Coreno, G. Crippa, G. De Ninno, M. Di Fraia, M. Galli, G. A. Garcia, Y. Mairesse, M. Negro, O. Plekan, P. Prasannan Geetha *et al.*, Time-resolved chiral x-ray photoelectron spectroscopy with transiently enhanced atomic site selectivity: A free-electron laser investigation of electronically excited fenchone enantiomers, Phys. Rev. X **13**, 011044 (2023).

[25] A. Kastner, T. Ring, B. C. Krüger, G. B. Park, T. Schäfer, A. Senftleben, and T. Baumert, Intermediate state dependence of the photoelectron circular dichroism of fenchone observed via femtosecond resonance-enhanced multi-photon ionization, J. Chem. Phys. **147**, 013926 (2017).

[26] S. Beaulieu, A. Comby, D. Descamps, B. Fabre, G. A. Garcia, R. Géneaux, A. G. Harvey, F. Légaré, Z. Mašín, L. Nahon, A. F. Ordonez, S. Petit, B. Pons, Y. Mairesse, O. Smirnova, and V. Blanchet, Photoexcitation circular dichroism in chiral molecules, Nat. Phys. **14**, 484 (2018).

[27] S. T. Ranecky, G. B. Park, P. C. Samartzis, I. C. Giannakidis, D. Schwarzer, A. Senftleben, T. Baumert, and T. Schäfer, Detecting chirality in mixtures using nanosecond photoelectron circular dichroism, Phys. Chem. Chem. Phys. **24**, 2758 (2022).

[28] A. Comby, D. Descamps, S. Petit, E. Valzer, M. Wloch, L. Pouységu, S. Quideau, J. Bocková, C. Meinert, V. Blanchet, B. Fabre, and Y. Mairesse, Fast and precise chiroptical spectroscopy by photoelectron elliptical dichroism, Phys. Chem. Chem. Phys. **25**, 16246 (2023).

[29] A. N. Artemyev, E. Kutscher, and P. V. Demekhin, Photoelectron circular dichroism of a model chiral anion, J. Chem. Phys. **156**, 031101 (2022).

[30] N. Mayer, S. Patchkovskii, F. Morales, M. Ivanov, and O. Smirnova, Imprinting chirality on atoms using synthetic chiral light fields, Phys. Rev. Lett. **129**, 243201 (2022).

[31] G. Gilat, Chiral coefficient—a measure of the amount of structural chirality, J. Phys. A: Math. Gen. **22**, L545 (1989).

[32] O. Neufeld, M. Even Tzur, and O. Cohen, Degree of chirality of electromagnetic fields and maximally chiral light, Phys. Rev. A **101**, 053831 (2020).

[33] O. Neufeld and O. Cohen, Unambiguous definition of handedness for locally chiral light, Phys. Rev. A **105**, 023514 (2022).

[34] E. Abraham and A. Nitzan, Molecular chirality quantification: Tools and benchmarks, J. Chem. Phys. **160**, 164104 (2024).

[35] S. Grimme, Continuous symmetry measures for electronic wavefunctions, Chem. Phys. Lett. **297**, 15 (1998).

[36] Y. Guo, D. Haase, J. Manz, H. Wang, and Y. Yang, Time-dependent extension of grimme's continuous chirality measure for electronic chirality flips in femto- and attosecond time domains, ChemPhysChem **25**, e202400132 (2024).

[37] A. F. Ordonez and O. Smirnova, Propensity rules in photoelectron circular dichroism in chiral molecules. I. Chiral hydrogen, Phys. Rev. A **99**, 043416 (2019).

[38] E. Kutscher, A. N. Artemyev, and P. V. Demekhin, Photoelectron circular dichroism in fenchone by short coherent broadband laser pulses, Phys. Rev. A **107**, 013107 (2023).

[39] G. Higgins, C. Zhang, F. Pokorny, H. Parke, E. Jansson, S. Salim, and M. Hennrich, Observation of second- and higher-order electric quadrupole interactions with an atomic ion, Phys. Rev. Res. **3**, L032032 (2021).

[40] K. Balzer, S. Bauch, and M. Bonitz, Efficient grid-based method in nonequilibrium Green's function calculations: Application to model atoms and molecules, Phys. Rev. A **81**, 022510 (2010).

[41] T. N. Rescigno and C. W. McCurdy, Numerical grid methods for quantum-mechanical scattering problems, Phys. Rev. A **62**, 032706 (2000).

[42] A. Scrinzi, t-SURFF: fully differential two-electron photoemission spectra, New J. Phys. **14**, 085008 (2012).

[43] V. Mosert and D. Bauer, Photoelectron spectra with Qprop and t-SURFF, Comput. Phys. Commun. **207**, 452 (2016).

[44] D. E. Manolopoulos, Derivation and reflection properties of a transmission-free absorbing potential, J. Chem. Phys. **117**, 9552 (2002).

[45] M. Edén and M. H. Levitt, Computation of orientational averages in solid-state NMR by Gaussian spherical quadrature, J. Magn. Reson. **132**, 220 (1998).

[46] See Supplemental Material at http://link.aps.org/supplemental/10.1103/PhysRevResearch.7.L012047 and references therein [49,50] for further details on the chirality measures and their evaluation as well as more detailed data and discussion regarding our numerical results.

[47] N. Weinberg and K. Mislow, On chirality measures and chirality properties, Can. J. Chem. **78**, 41 (2000).

[48] G. F. von Rudorff, A. N. Artemyev, B. M. Lagutin, and P. V. Demekhin, Optimal photoelectron circular dichroism of a model chiral system, J. Chem. Phys. **160**, 214301 (2024).

[49] S. T. Manson and A. F. Starace, Photoelectron angular distributions: energy dependence for *s* subshells, Rev. Mod. Phys. **54**, 389 (1982).

[50] R. Mehrem and A. Hohenegger, A generalization for the infinite integral over three spherical bessel functions, J. Phys. A **43**, 455204 (2010).

[51] C. Lux, M. Wollenhaupt, C. Sarpe, and T. Baumert, Photoelectron circular dichroism of bicyclic ketones from multiphoton ionization with femtosecond laser pulses, ChemPhysChem **16**, 115 (2015).